Electronic Supplementary Material (ESI) for Journal of Materials Chemistry A.
This journal is © The Royal Society of Chemistry 2021

Supporting Information

Highly Conjugated Three-Dimensional Covalent Organic Frameworks with Enhanced Li-ion Conductivity as Solid-State Electrolytes for High-Performance Lithium Metal Batteries

Shi Wang,[a†] *Xiangchun Li,*[a†] *Tao Cheng,*[a†] *Yuanyuan Liu,*[a] *Qiange Li,*[a] *Minglei Bai,*[a] *Xu Liu,*[a] *Haigang Geng,*[a] *Wen-Yong Lai,*[ab]* *and Wei Huang*[ab]

[a] *State Key Laboratory of Organic Electronics & Information Displays (SKLOEID), Institute of Advanced Materials (IAM), Nanjing University of Posts & Telecommunications, 9 Wenyuan Road, Nanjing 210023, China.*

[b] *Frontiers Science Center for Flexible Electronics (FSCFE), MIIT Key Laboratory of Flexible Electronics (KLoFE), Northwestern Polytechnical University, Xi'an 710072, China.*

[†] *Shi Wang, Xiangchun Li and Tao Cheng contributed equally to this work.*

E-mail: iamwylai@njupt.edu.cn

EXPERIMENTAL SECTION

Materials

Succinonitrile (SN) and bis(trifluoromethane)sulfonimide lithium (LiTFSI) were received from Aladdin and used directly. Terephthalaldehyde (Aladdin, 98%), 2,2',7,7'-Tetrabromo-9,9'-spirobifluorene (aladdin, 98%), 4-aminophenylboronic acid pinacol ester (aladdin, 98%) and acetic acid (aladdin, 99.7%) were used as received. Orthodichlorobenzene (AR, Sinopsin group chemical reagent co. LTD) and *n*-butanol (AR, Sinopsin group chemical reagent co. LTD) were dried by CaH_2 and then distilled before use. All other materials were used directly unless otherwise stated.

Experiment

Characterization

^1H NMR and ^{13}C NMR spectra were conducted on a Bruker Ultra Shield Plus 400MHz NMR. The molecular weight of intermediate was recorded *via* a Bruker matrix-assisted laser desorption/ionization time of flight mass spectrometry (MALDI-TOF MS). Gas adsorption analyzer (V-Sorb 2800P, Gold APP Corp., Beijing, China) was used to obtain the N_2 adsorption-desorption isotherm. Thermal stability analyses were performed on a thermal gravimetric analyzer (NETZSCH TG 209F3) from 30 to 600ºC with the heating rate of 20ºC min^{-1}. Fourier transform infrared (FTIR) spectra were conducted on a Thermo Nicolet AVATAR 360 infrared instrument using the attenuated total reflectance (ATR) technique from 3200 to 1000 cm^{-1}. ^7Li Solid-state NMR spectra were acquired on a Bruker Avance III HD500m, the ^7Li chemical shift was referenced to solid LiCl at 0 ppm. The NMR measurements were performed at room temperature. SEM images were performed using a Field Emission Scanning Electron Microscope (FESEM, Hitachi SU8010). The samples were sputtered with Au for 30 s. Transmission electron microscope (TEM, JEOL 2010) was used to record the TEM images at an accelerating voltage of 100 kV. In addition, XRD tests were performed on Bruker D8 advance with a copper target (λ =1.54 Å).

Electrochemical measurements

The symmetric Li/COF-based SSEs/Li cells were used for lithium plating/striping experiments, which were conducted on a LANHE CT2001A battery testing system with charge/discharge times of 1 h at ambient temperature. In addition, the ionic conductivity of the samples was obtained *via* EIS, the t^+ of the samples was calculated according to the potentiostatic polarization method, and the electrochemical stability of samples was tested using linear sweep voltammetry. Detailed methods can be found in our previous reports.[S1-3]

Preparation of $LiFePO_4$ electrode: $LiFePO_4$ (70 mg) and Super-P (20 mg) were weighed and mixed in a mortar and pestle, then PVDF (10 mg) was added, thoroughly mixed and ground, and finally NMP (0.5 mL) was added, well infiltrated and continued to be ground to a homogeneous slurry. The slurry was casted onto an aluminum foil, blown at 80°C for 4 h, dried under vacuum at 120°C for 12 h, and cut to obtain electrode sheets.

Preparation of $Li_4Ti_5O_{12}$ electrode: The procedure of preparing $Li_4Ti_5O_{12}$ electrode is the same as that of preparing $LiFePO_4$.

Preparation of $LiCoO_2$ electrode: The procedure of preparing $LiCoO_2$ electrode is the same as that of preparing $LiFePO_4$, except that the ratio of $LiCoO_2$, super-P and PVDF becomes 90:5:5.

Preparation of all-solid-state cells: The all-solid-state lithium metal cells were obtained by stacking and encapsulating the cathode, COF electrolytes (COF powder was cold pressed at 10 Mpa to obtain a self-standing film and placed on the cathode, and then 5 μL of SN/30 wt% LiTFSI was added dropwise to obtain the COF electrolyte), lithium metal anode, stainless steel sheet and shrapnel in a

2025 coin cell case from the bottom up.

In addition, LFP/COF-based electrolyte/Li and LCO/COF-based electrolyte/Li cells were assembled in an Ar-filled glovebox (MB-Labstar 1200/780, both H_2O and O_2 contents lower than 0.5 ppm) to assess the cell performance. Both LFP and LCO were provided by Pulead Technology Industry Co., Ltd. The active substance content was 1.5-2.5 mg cm^{-2} for LFP-based cathode and 3~4 mg cm^{-2} for LCO-based cathode. Moreover, the cell performance evaluation of all the cells was conducted on a LANHE CT2001A battery testing system. The voltage range for the LFP/SSE/Li cells was between 2.5 to 4 V at AT, while the voltage range for the LCO/SSE/Li cells was between 4.3 to 2 V at AT.

Theoretical calculation details

All the density-functional theory (DFT) computations were performed using the $Dmol^3$ software package based on the linear combination of atomic orbitals (LCAO) method. Electron-ion interactions were described using the DFT Semi-core Pseudopots (DSPP) pseudopotentials. A double numerical polarized (DNP) basis set was employed to expand the wave functions with an orbital cutoff of 3.3 Å for O, 3.1 Å for H, 3.7 Å for C, 3.4 Å for N 5.1 Å for Li. For the electron-electron exchange and correlation interactions, the function parametrized by Perdew-Burke-Ernzerhof (PBE), a form of the general gradient approximation (GGA), was used throughout. The vander Waals interactions were described using DFT-D2 method that proposed by Grimme.

During the geometry optimizations, the atoms far from the reaction center were fixed at the bulk position. The convergence criterion for the electronic self-consistent field (SCF) loop was set to 10^{-5}. The atomic structures were optimized until the residual forces were below 0.004 Ha $Å^{-1}$. The transition state search was conducted *via* the quadratic synchronous transit (QST) method, and the tolerance for RMS of force was set to 0.004 Ha $Å^{-1}$.

Synthesis of 3D-SpCOFs

The synthesis of 3D-SpCOF and 3D-SpCOF-OH was conducted according to the procedures reported in our previous work.[S4] Sp-4(Ph-NH_2) was synthesized as follows: 4-aminophenylboronic acid pinacol ester (4.382 g, 20.0 mmol), 2,2',7,7'-tetrabromo-9,9'-spirobifluorene (2.528 g, 4.0 mmol), tetrabutylammonium bromide (TBAB) (0.69 g, 10 wt%), K_2CO_3 (aq., 4 M, 40 mL) and toluene (70 mL) were mixed and degassed, then $Pd(PPh_3)_4$ was added. The mixture was refluxed under N_2 for 72 h. Subsequently, toluene was removed by rotary evaporator. Then distilled water (200 mL) was poured into the mixture and extracted with 200 mL ethyl acetate (EA) for 3 times. After the sample was dried using anhydrous Na_2SO_4, the crude product was purified by Alumina-B column chromatography using PE/EA (1:4) as eluent. Subsequently, a grayish-white solid was obtained after evaporation of the solvent. Finally, white powder of 4,4',4'',4'''-(9,9'-spirobifluorene-2,2',7,7'-tetrayl)tetraaniline (Sp-4(Ph-NH_2)) was obtained in ~72% yield by recrystallization from *n*-hexane (see the ^{1}H NMR, ^{13}C NMR and MALDI-TOF characterizations of the sample in Figure S1 and S2, respectively).

By condensing of Sp-4(Ph-NH_2) (39.0 mg, 0.105 mmol) and terephthalaldehyde (28 mg, 0.21 mmol) in the mixture of orthodichlorobenzene/*n*-butanol/acetic acid (volume ratio of 7:3:1) at 120°C for 72 h, the 3D-SpCOF was obtained as yellow powder (insoluble in common organic solvents).

3D-SpCOF-OH was synthesized similarly by using 2,5-dihydroxyterephthalaldehyde instead of terephthalaldehyde.

Preparation of 3D-SpCOF SSEs

The 3D-SpCOF SSEs were prepared *via* cold-pressing method, then SN/LiTFSI was embedded into COFs *via* drip coating. Specifically, the COF electrolytes were prepared by pipetting ~10 µL of SN (mass ratio of SN and LiTFSI was 10:3) directly onto the COF films, which were done in a glove box at room temperature. The mass of the COF films was about 25 mg, while the mass ratio of COF pellet and LiTFSI was about 4:1. The volume of the film is calculated to be about 0.055 cm^3, while the density of COF pellets is about 0.45 g cm^{-3} and the density of COF-SN/LiTFSI is about 0.95 g cm^{-3}.

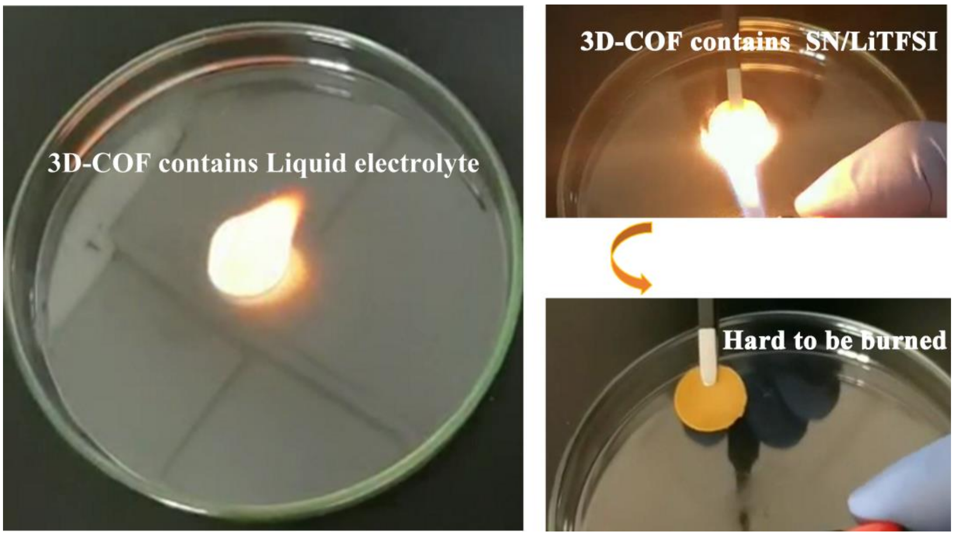

Figure S1. Combustion experiments of 3D-SpCOF containing liquid electrolyte (the content of liquid electrolyte is the same as SN) and 3D-SpCOF-SSE.

Note: Figure S1 show the combustion experiments of 3D-SpCOF containing liquid electrolyte (1.0 M $LiPF_6$ in EC:DEC:EMC=1:1:1 Vol%, the content of liquid electrolyte is the same as SN) and 3D-SpCOF-SSE. Obviously, 3D-SpCOF containing liquid electrolyte exhibits higher flammability than 3D-SpCOF-SSE. This is because the liquid electrolyte is extremely combustible, while SN shows low flammability.

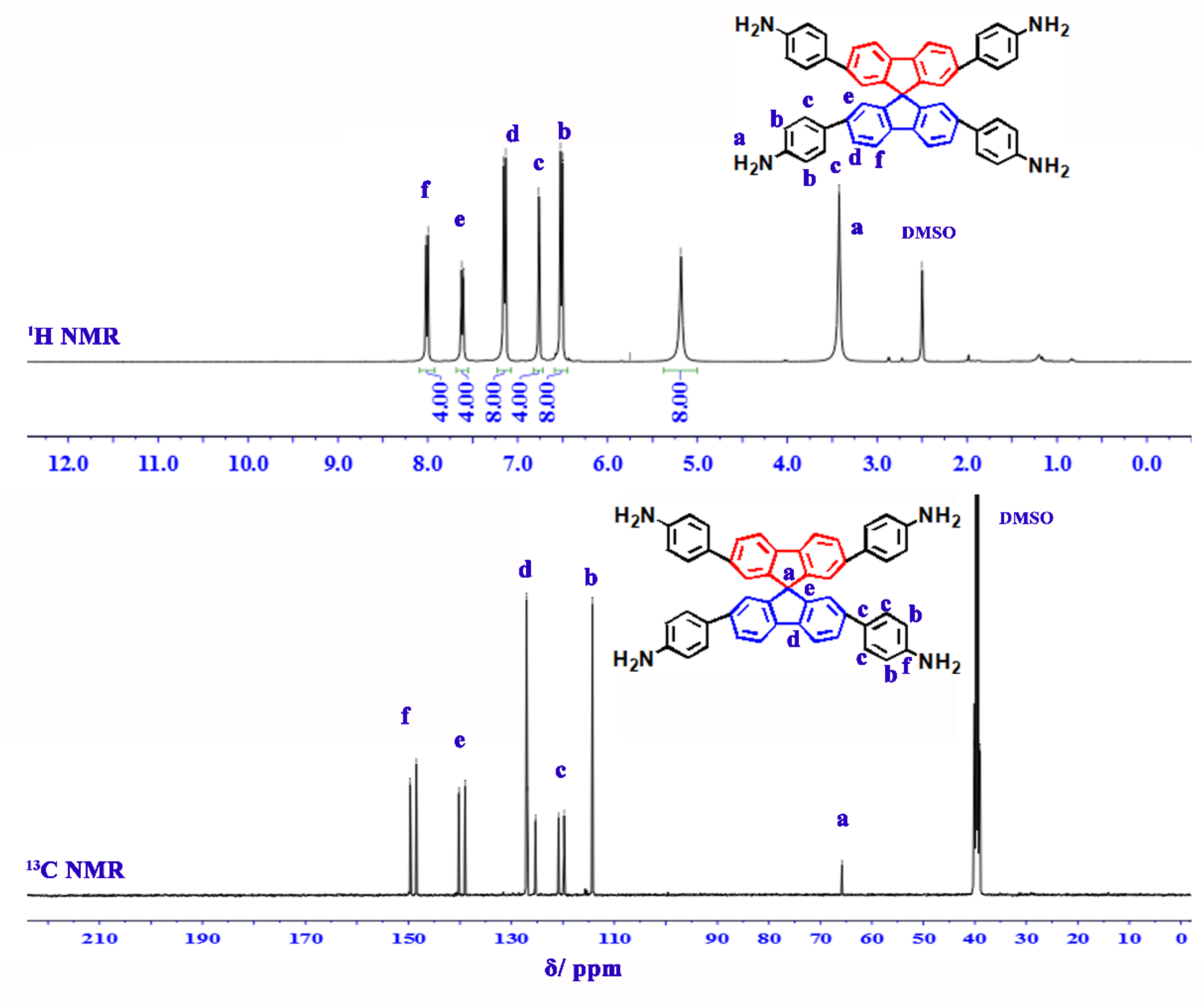

Figure S2. ^{1}H NMR and ^{13}C NMR for 4,4',4'',4'''-(9,9'-spirobifluorene-2,2',7,7'-tetrayl)tetraaniline.

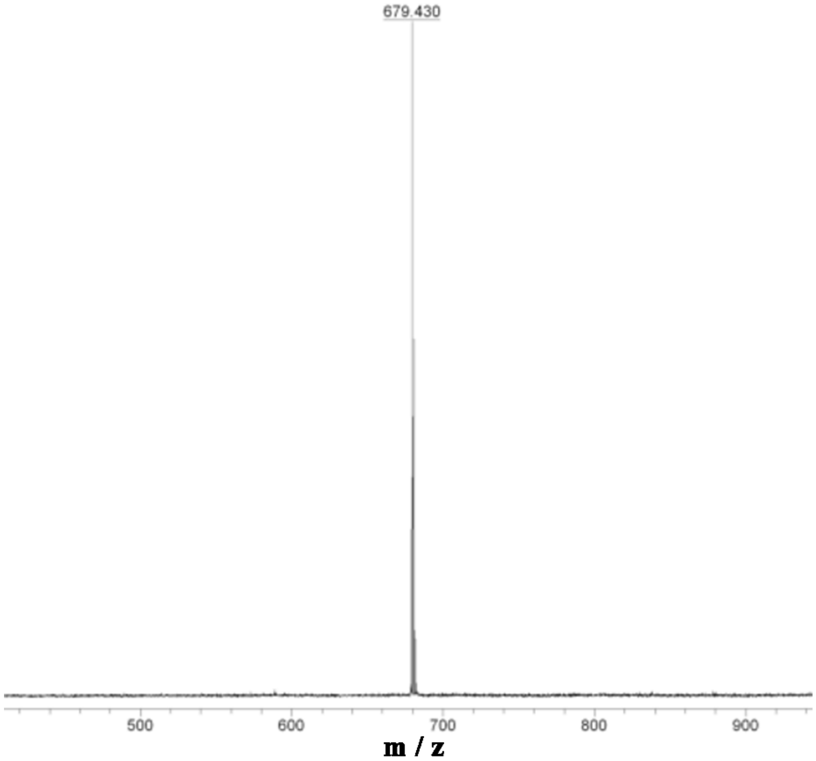

Figure S3. MALDI-TOF for 4,4',4'',4'''-(9,9'-spirobifluorene-2,2',7,7'-tetrayl)tetraaniline.

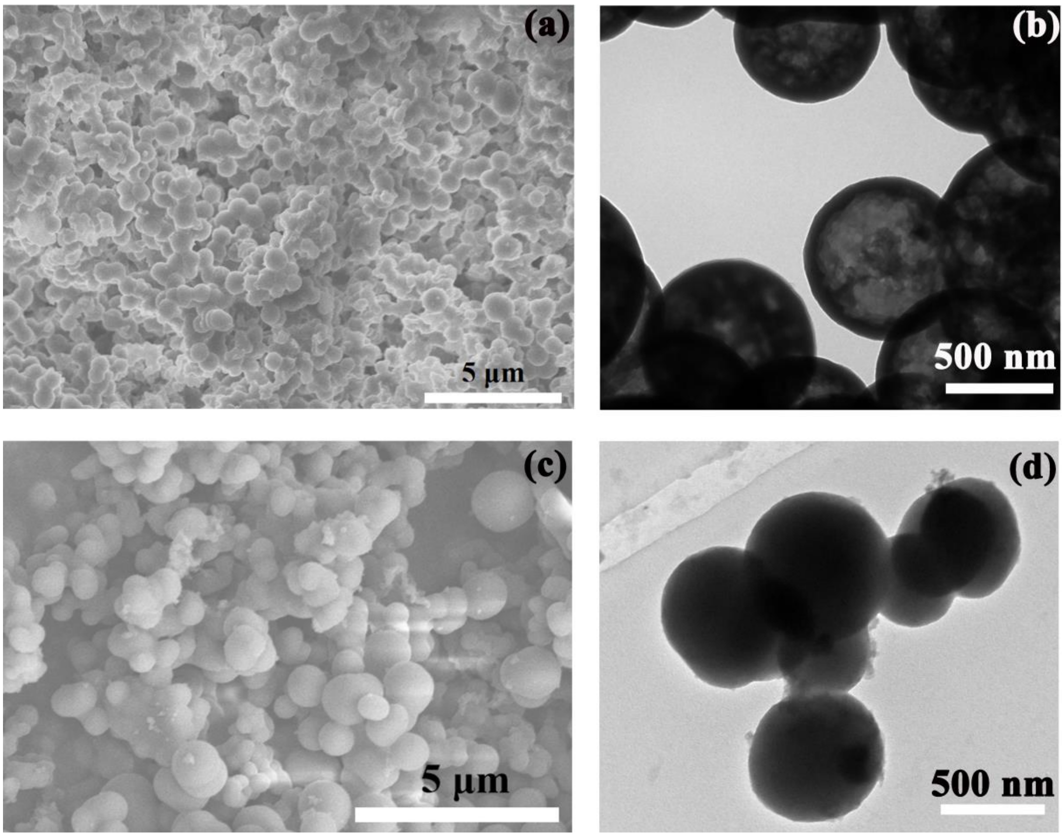

Figure S4. SEM (a) and TEM (b) images of 3D-SpCOF, respectively. (c) and (d) show the SEM and TEM images of 3D-SpCOF-OH, respectively.

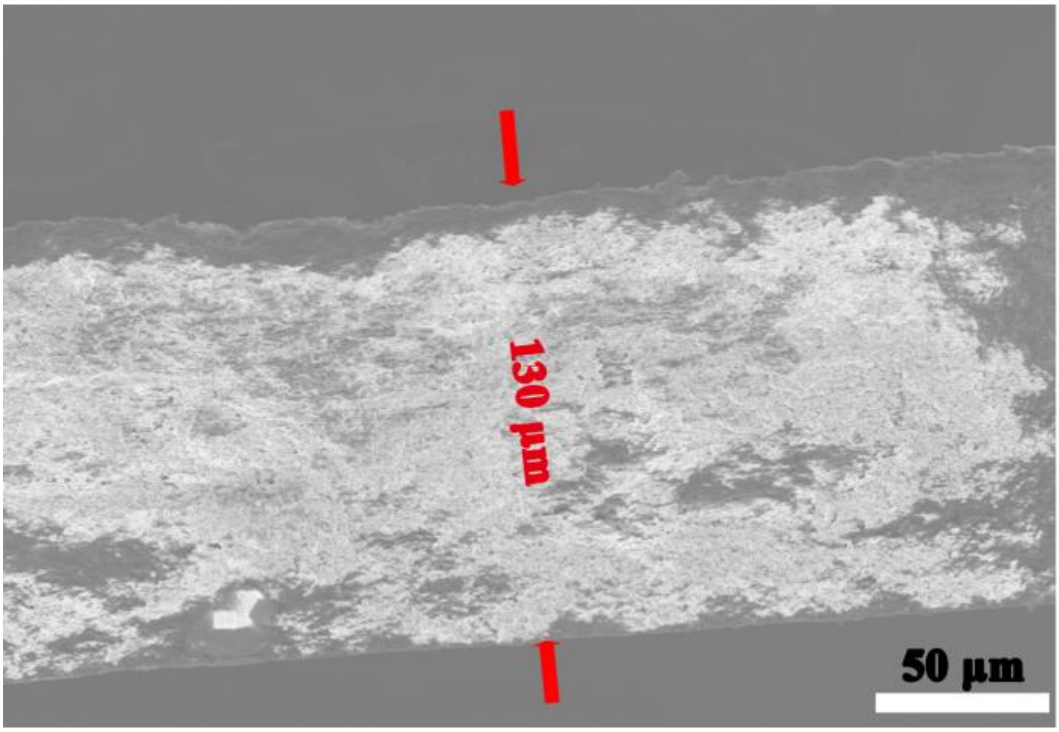

Figure S5 Cross section SEM image of the free-standing 3D-SpCOF film; the bright white is likely due to the uneven deposition of gold.

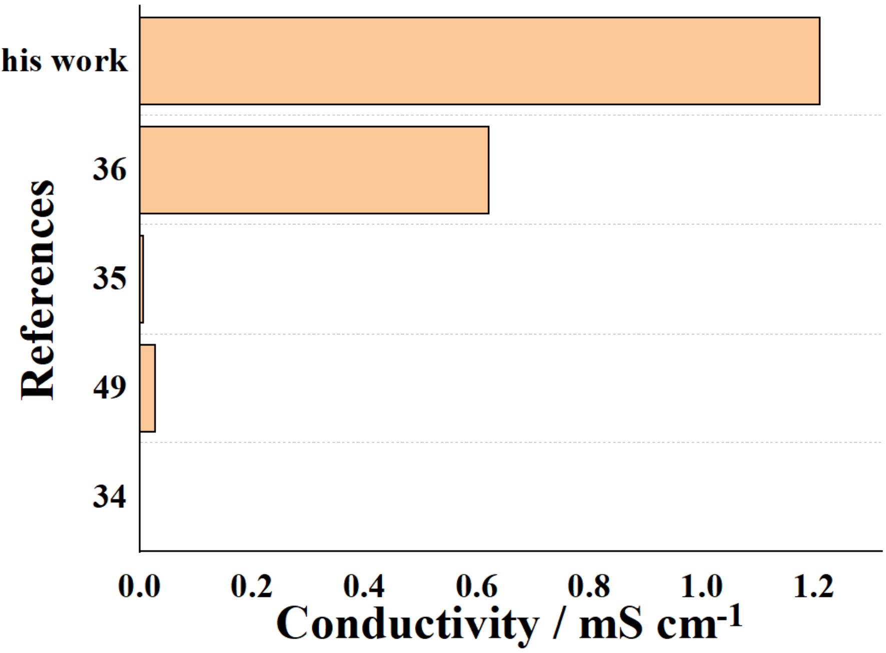

Figure S6. Ionic conductivity of 3D-SpCOF-SSE as compared with those reported in the references listed in the manuscript.

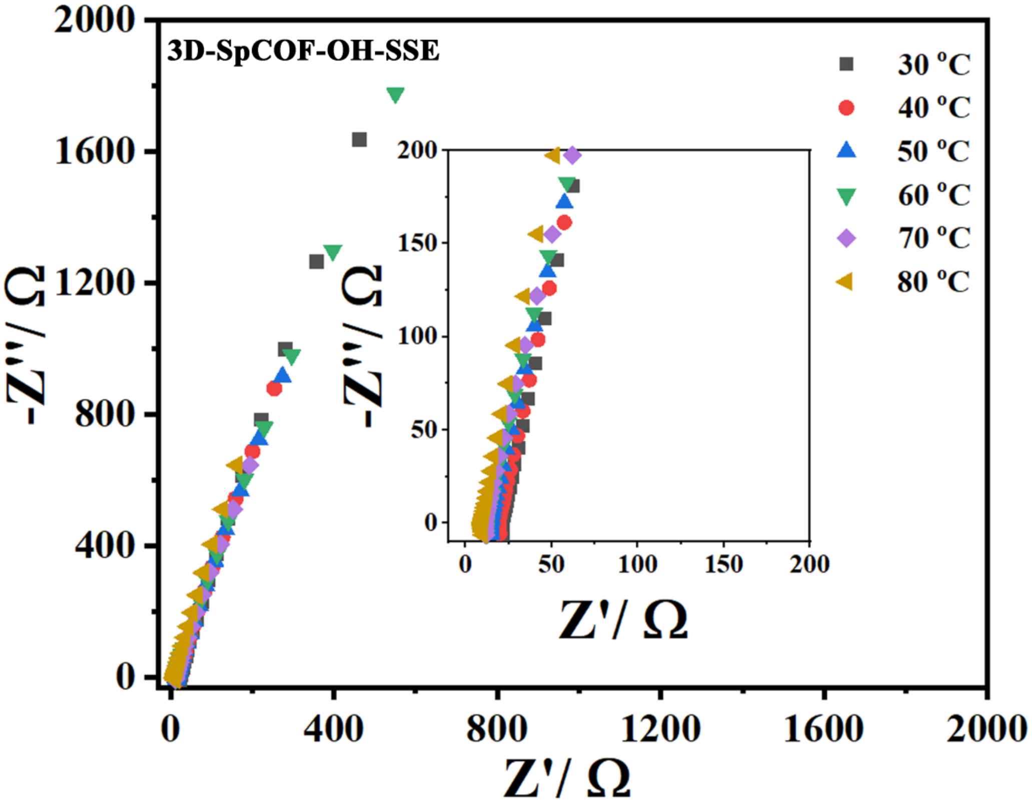

Figure S7. EIS of 3D-SpCOF-OH-SSE at different temperatures.

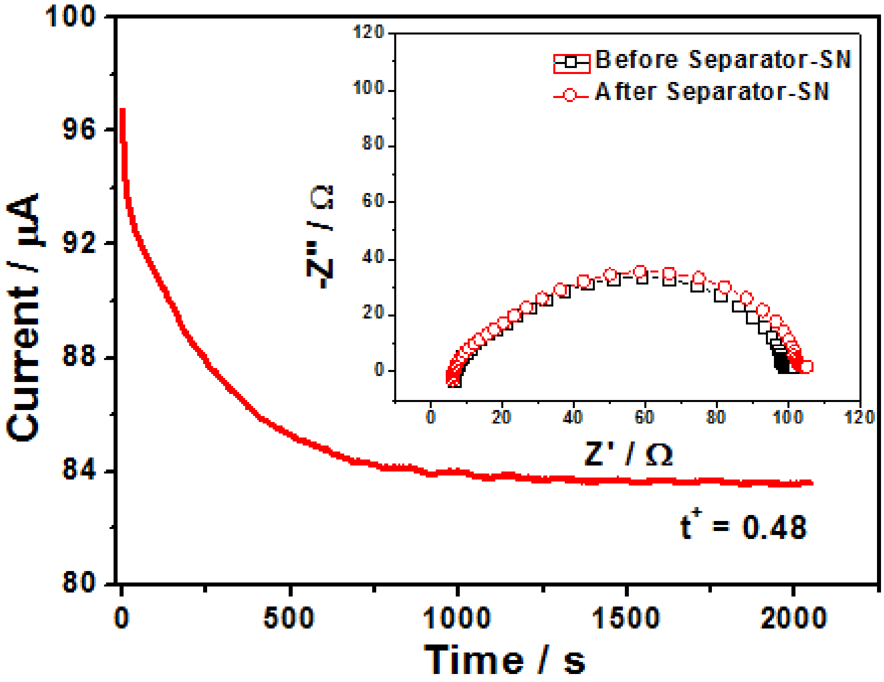

Figure S8. The chronoamperometry of the Li/SN-PE separator/Li symmetric cell (experiment condition: AT, potential step of 10 mV). The insets present the EIS before and after polarization at ambient temperature.

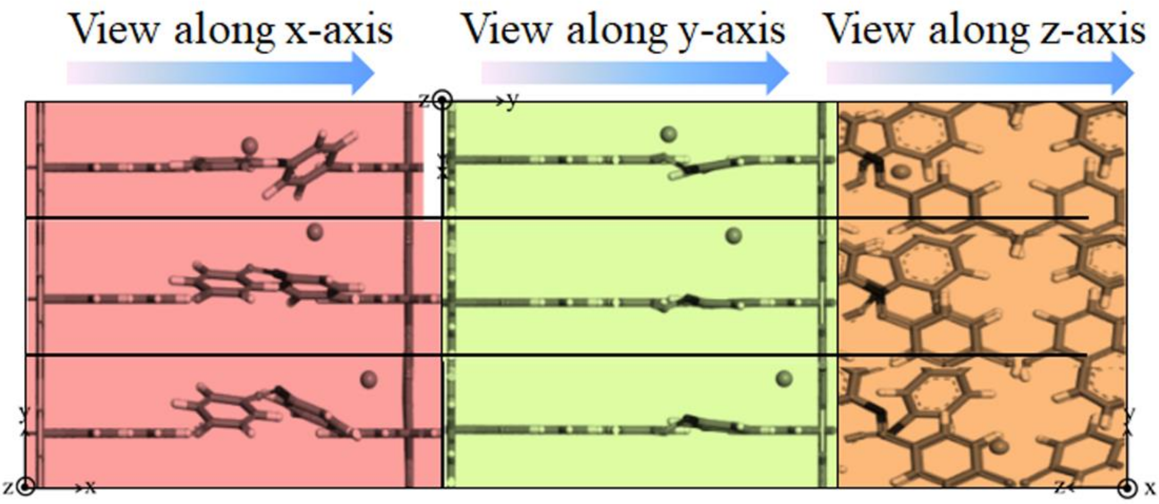

Figure S9. Theoretical elucidation of Li^+ migration behaviors inside the COF channels. It shows the initial, intermediate and final states view along X, Y and Z axis of 3D-SpCOF/Li^+, respectively.

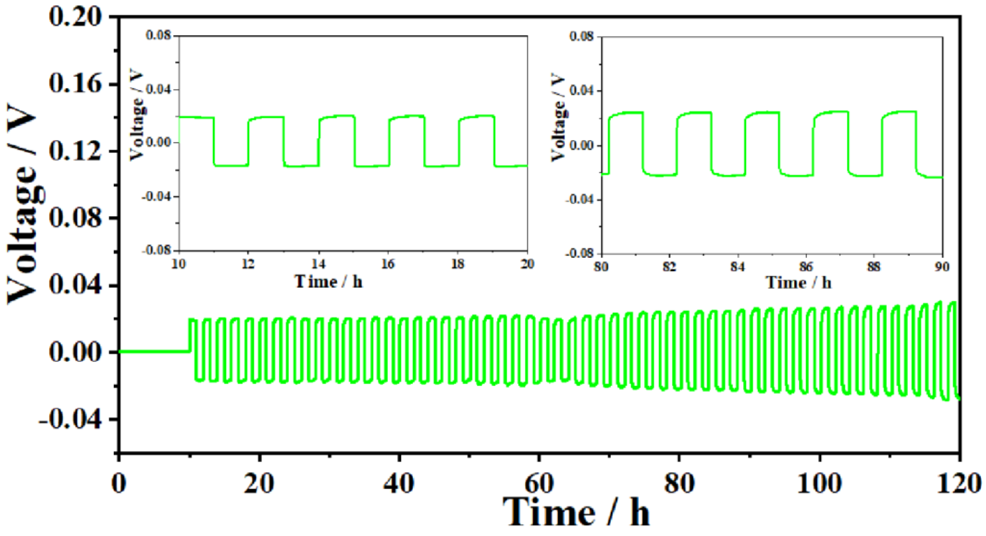

Figure S10. Li plating/stripping experiment of Li/3D-SpCOF-SSE/Li cell at current density of 0.12 mA cm^{-2}.

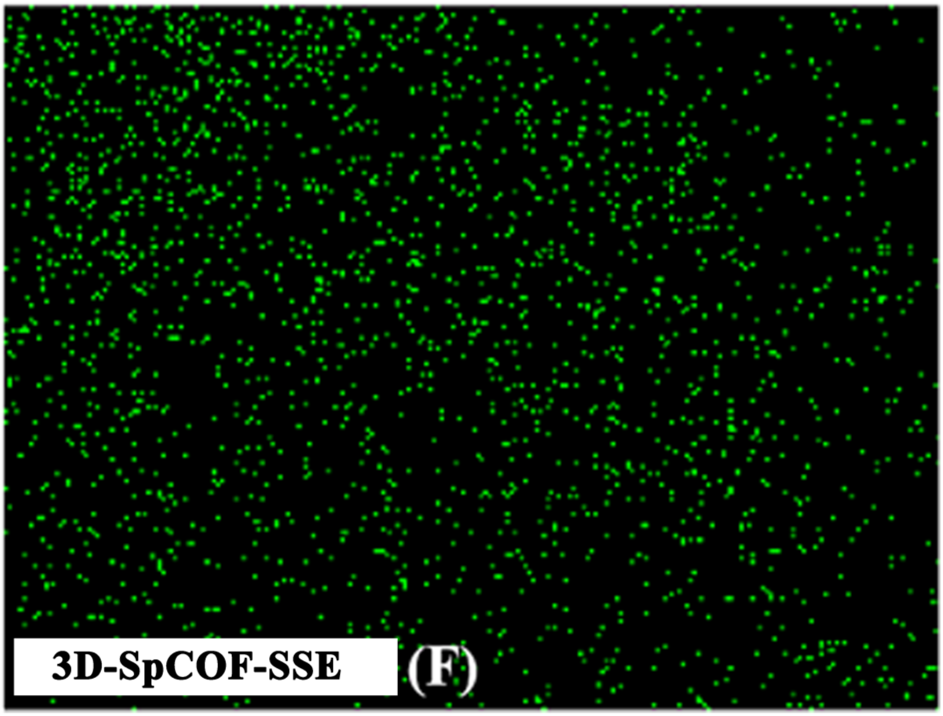

Figure S11. EDS elemental mapping of F for 3D-SpCOF-SSE,

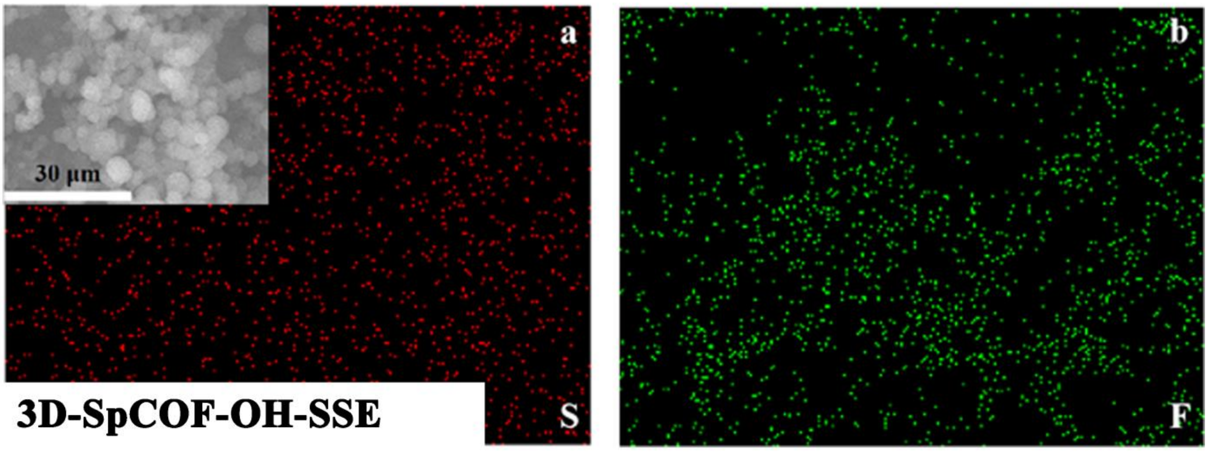

Figure S12. (a) and (b) show the EDS elemental mappings of S and F for 3D-SpCOF-OH-SSE, respectively; inset of Figure S11a presents the corresponding SEM image.

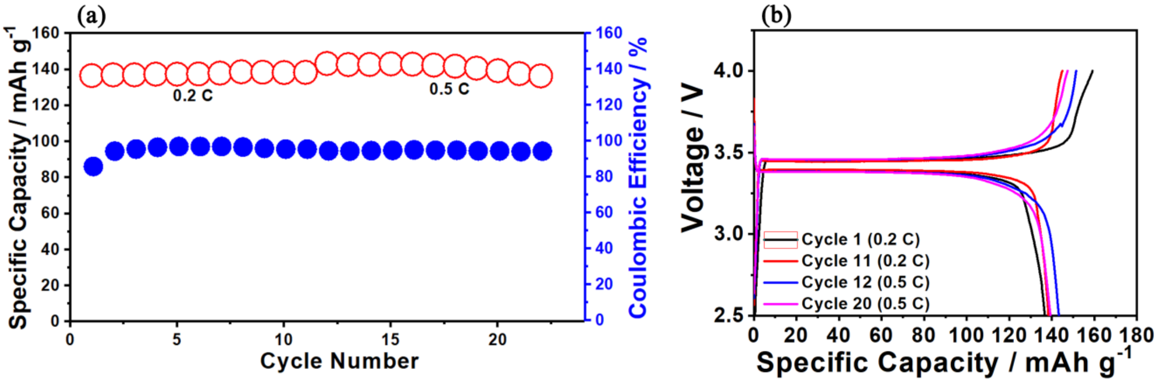

Figure S13. (a) Cycling performance of the Li/3D-SpCOF-SSE/LFP cell at 0.2 and 0.5 C. (b) The corresponding charging/discharge curves at 0.2 and 0.5 C.

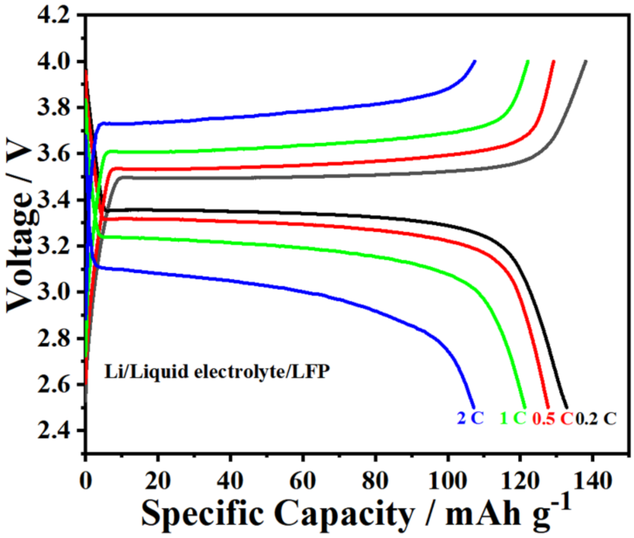

Figure S14. Charge-discharge curves of Li/LFP cell using liquid electrolyte under current densities of 0.2, 0.5, 1 and 2C.

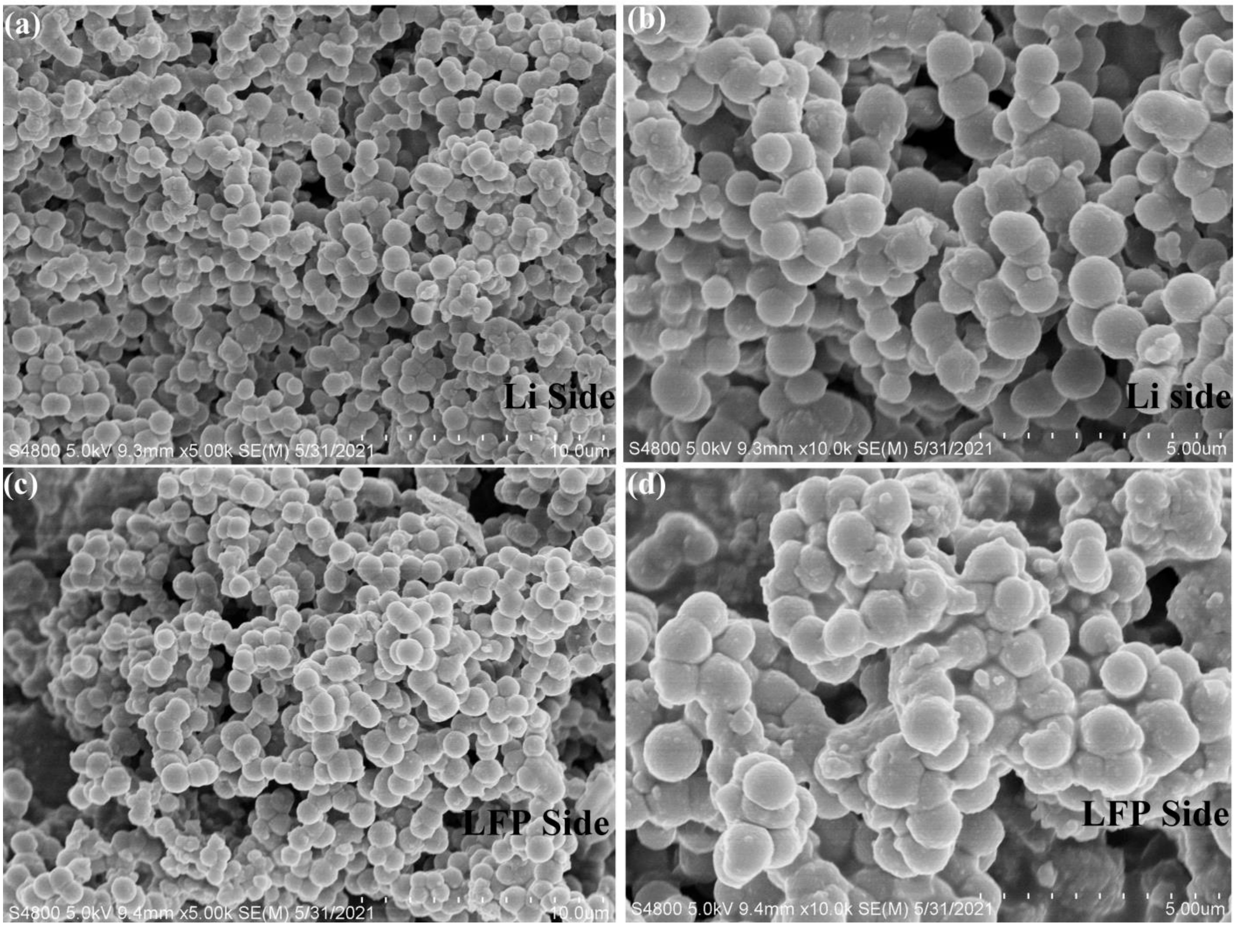

Figure S15. SEM images of 3D-SpCOF-SSE after cycling. (a) and (b) show the surface images of electrolyte at Li anode side, while (c) and (d) are the surface images of electrolyte at LFP cathode side.

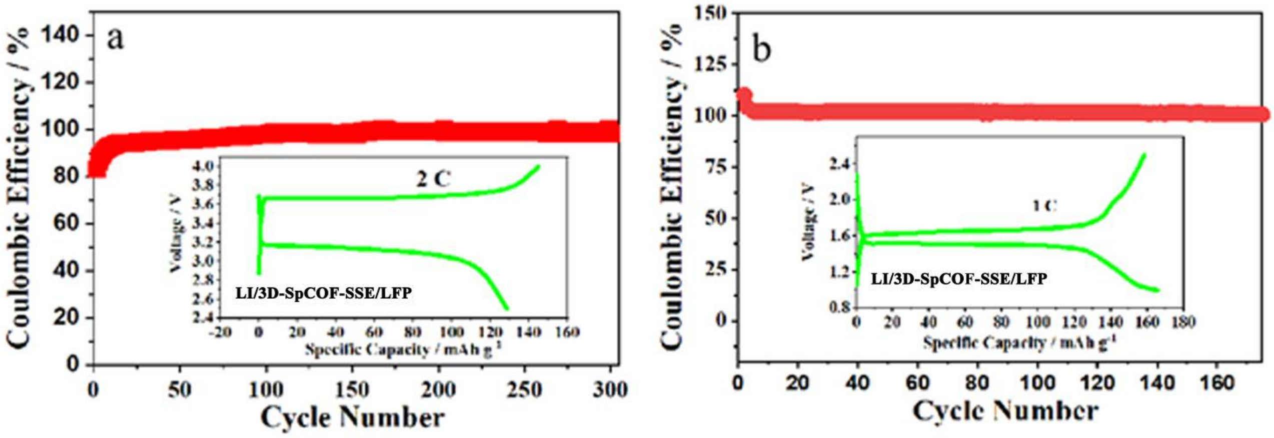

Figure S16. Coulombic efficiency of (a) Li/LFP and (b) Li/$Li_4Ti_5O_{12}$ (LTO) cells using 3D-SpCOF-SSE at 2C and 1 C, respectively, the inset shows the corresponding charging/discharge curves.

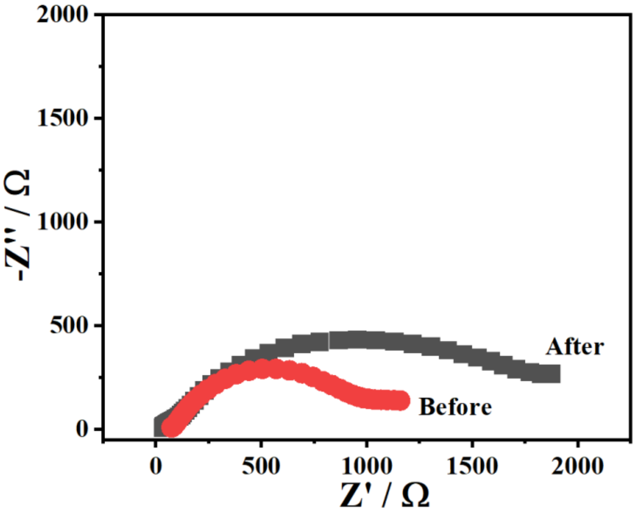

Figure S17. ESI of Li/3D-SpCOF-SSE/LFP cell before and after cycling.

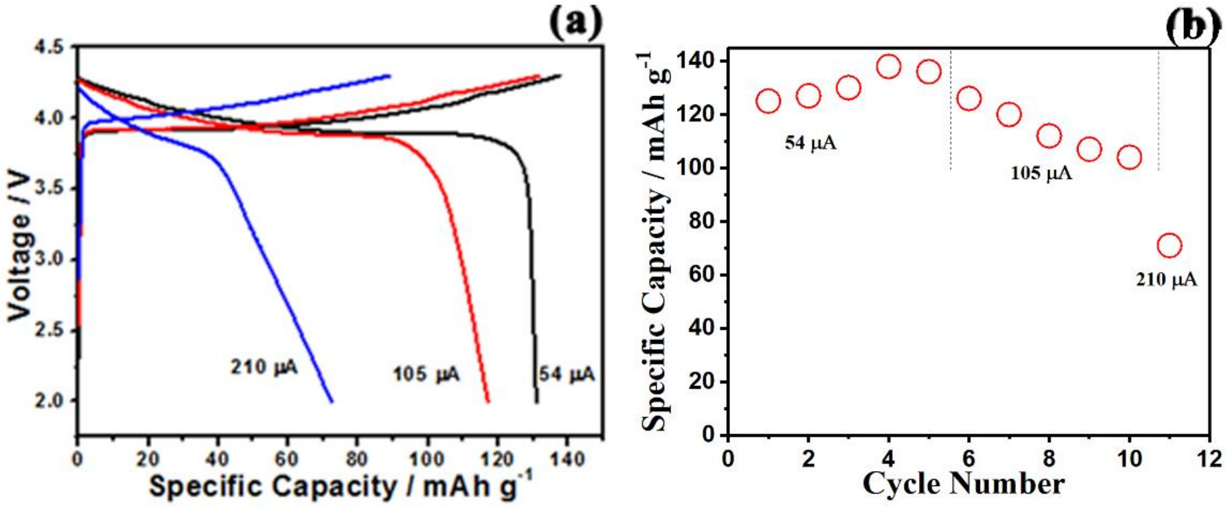

Figure S18. (a) Charge-discharge curves of the Li/3D-SpCOF-SSE/LCO cell at different current densities (also see it in our previous work[S4]). (b) Cycle performance of the cell. The experiment was conducted at ambient temperature.

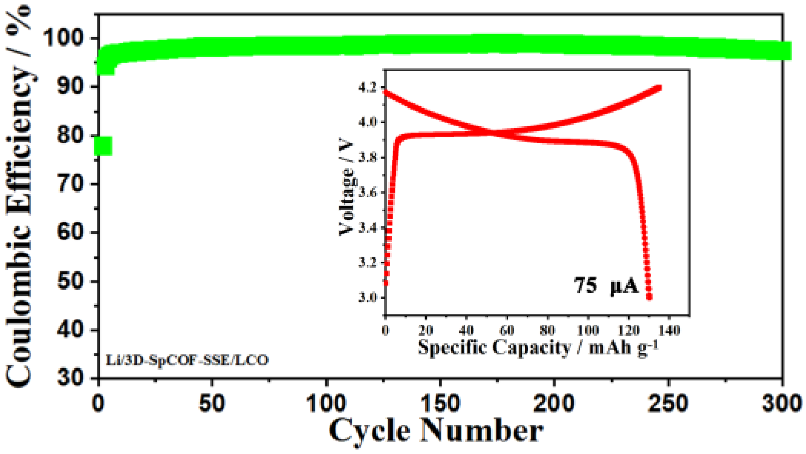

Figure S19. Coulombic efficiency of Li/3D-SpCOF-SSE/LCO cell for 300 cycles and the corresponding charge/discharge curves

Table S1. Comparison of ionic conductivity of the 3D-SpCOF-based solid-state electrolytes with other ones in the references

Samples	*Ionic conductivity ($S\ cm^{-1}$)*	References
PEG-Li^+@CD-COF-Li	2.6×10^{-5} (30°C)	S5
ICOF-2:PVDF	3.05×10^{-5}(RT)	S6
Im-COF-TFSI@Li	2.92×10^{-5} (30°C)	S7
Li+@TPB-DMTP-COF	1.36×10^{-7} (40°C)	S8
TpPa-SO_3Li	2.7×10^{-5} (RT)	S9
COF-PEO-6-Li	6.25×10^{-10} (RT)	S10
3D-SpCOF-SSE	6.4×10^{-4} (30°C)	This work
3D-SpCOF-OH-SSE	1.3×10^{-3} (30°C)	This work

Table S2. Related parameters and t^+ of the related electrolytes

Samples	R_{lo} (Ω)	R_{ls} (Ω)	I_o (μA)	I_s (μA)	t_{Li}^+
SN/LiTFSI	*93*	*98*	*96.7*	*83.6*	*0.48*
3D-SpCOF-OH-SSE	144	151	55.7	48.4	0.64
3D-SpCOF-SSE	88	86	82.7	74.7	0.7

References:

S1. S. Wang, Q. Zeng, A. Wang, X. Liu, J. Chen, Z. Wang, L. Zhang, *J. Mater. Chem. A* 2019, **7**, 1069-1075.

S2. L. Zhang, S. Wang, J. Li, X. Liu, P. Chen, T. Zhao, L. Zhang, *J. Mater. Chem. A* 2019, **7**, 6801-6808.

S3. S. Wang, X. Liu, A. Wang, Z. Wang, J. Chen, Q. Zeng, X. Jiang, H. Zhou, L. Zhang, *ACS Appl. Mater. Interfaces* 2018, **10**, 25273-25284.

S4. Y.-Y. Liu, X.-C. Li, S. Wang, T. Cheng, H. Yang, C. Liu, Y. Gong, W.-Y. Lai, W. Huang, *Nat. Commun.,* 2020, **11**, 5561.

S5. Z. Guo, Y. Zhang, Y. Dong, J. Li, S. Li, P. Shao, X. Feng, B. Wang, *J. Am. Chem. Soc.,* 2019, **141**, 1923-1927.

S6. Y. Du, H. Yang, J. M. Whiteley, S. Wan, Y. Jin, S. Lee, W. Zhang, *Angew. Chem.,* 2016, **55**, 1737-1741.

S7. Z. Li, Z.-W. Liu, Z.-J. Mu, C. Cao, Z. Li, T.-X. Wang, Y. Li, X. Ding, B.-H. Han, W. Feng, *Mater. Chem. Front.,* 2020, **4**, 1164-1173.

S8. Q. Xu, S. Tao, Q. Jiang, D. Jiang, *J. Am. Chem. Soc.,* 2018, **140**, 7429-7432.

S9. K. Jeong, S. Park, G. Y. Jung, S. H. Kim, Y.-H. Lee, S. K. Kwak, S.-Y. Lee, *J. Am. Chem. Soc.,* 2019, **141**, 5880-5885.

S10. G. Zhang, Y.-L. Hong, Y. Nishiyama, S. Bai, S. Kitagawa, S. Horike, *J. Am. Chem. Soc.,* 2019, **141**, 1227-1234.